Adaptive Stabilization for Uncertain Nonholonomic Dynamic Mobile Robots Based on Visual Servoing Feedback

YANG Fang[1, 2] WANG Chao-Li[1]

Abstract The stabilization problem of nonholonomic dynamic mobile robots with a fixed (ceiling-mounted) camera is addressed in this paper. First, a camera-object visual servoing kinematic model is introduced by utilizing the pin-hole camera model and a kinematic stabilizing controller is given for the kinematic model. Then, an adaptive sliding mode controller is designed to stabilize uncertain dynamic mobile robot in the presence of parametric uncertainties associated with the camera system. The proposed controller is robust not only to structured uncertainty such as mass variation but also to unstructured one such as disturbances. The stability of the proposed control system and the boundedness of estimated parameters are rigorously proved by Lyapunov method. Simulation results are presented to illustrate the performance of the control law.

Key words Nonholonomic mobile robots (NMR), stabilization, adaptive control, visual servoing

DOI 10.3724/SP.J.1004.2011.00857

Over the past ten years, the control of nonholonomic systems have formed an active area within the nonlinear control community. By the theorem of Brockett[1], a nonholonomic system cannot be stabilized at a single equilibrium point by any continuous, time-invariant, state-feedback controller. To solve this problem, lots of methods have been considered[2−7]. In the control of nonholonomic mobile robots, it is usually assumed that the robot states are available and exactly reconstructed using proprioceptive and exteroceptive sensor measurements. Unfortunately, in real-world applications involving mobile robots, these assumptions often do not hold due to uncertainties in the kinematic and dynamic models, mechanical limitations and measurement noise. As a consequence, the estimation of the robot states from sensor measurements can be affected by these perturbations. An interesting approach to overcome this position measurement problem is to utilize a vision system to directly obtain the Cartesian position information required by the controller.

Since the late 1980 s, much effort has been made into visual servoing and vision-based manipulations[8−11]. A significant issue with camera-based vision systems is the lack of depth information. From a review of literature, various approaches have been developed to address the lack of depth information inherent in vision systems. Chen et al.[12] developed a mobile robot visual servoing tracking controller when a monocular camera was onboard. In [13], asymptotic regulation of the position/orientation of a mobile robot with a monocular camera was achieved by exploiting homography-based visual servoing control strategies. However, the homography estimation and decomposition process were not a trivial issue. Wang et al.[14] investigated the dynamic feedback robust stabilization of nonholonomic mobile robots with uncalibrated monocular camera based on visual servoing feedback.

The methods mentioned above are based on kinematics only and the nonlinear forces in robot dynamics are neglected. However, in practice, it is more realistic to formulate the nonholonomic system control problem at dynamic level, where the torque and force are taken as the control inputs. Liu et al.[15] presented a new adaptive controller for image-based dynamic control of a robot manipulator using a fixed camera whose intrinsic and extrinsic parameters were not known. [16] proposed a new adaptive controller for image-based visual servoing of both point and line features using an uncalibrated eye-in-hand camera system. Dixon et al.[17] used feedback from an uncalibrated, fixed (ceiling-mounted) camera to present an adaptive tracking controller for a mobile robot that compensated for the parametric uncertainties in the camera and the mobile robot dynamics. However, the development in [17] cannot be applied to the mobile robot stabilization problem due to restrictions on the mobile robot reference velocity (i.e., the reference linear velocity does not converge to zero).

In this paper, the stabilization problem of a nonholonomic mobile robot (NMR) with uncertain dynamics and uncertain visual parameters is considered. Specifically, an adaptive sliding mode controller is proposed for the NMR, in which adaptive control techniques are used to compensate for the parametric uncertainties and sliding mode control is used to suppress the bounded disturbances. The controller guarantees the output of the dynamic subsystem (the input of the kinematic subsystem) to track some bounded auxiliary signals which subsequently drive the kinematic subsystem to achieve global asymptotic stabilization. The most interesting feature of this paper is that the problem is discussed in the image frame and the inertial frame, which make the problem easy and useful.

This paper is organized as follows. In Section 1, based on the pin-hole camera model, the camera-object visual servo kinematic and dynamic models of an NMR are introduced. In Section 2, a kinematic stabilizing controller and a torque controller for the NMR are developed. In Section 3, the dynamic stability of the proposed controller is rigorously proved by the Lyapunov method. In Section 4, the controller′s performance is illustrated through the simulation results. The last section presents a conclusion and outlines the future work.

1 Problem formulation

1.1 Kinematic and dynamic models

A typical example of a nonholonomic mobile robot is shown in Fig.1. The two rear wheels of the robot are controlled independently by motors, and a front castor wheel prevents the robot from tipping over as it moves on a plane.

Manuscript received July 1, 2010; accepted March 2, 2011
Supported by National Natural Science Foundation of China(60874002), Key Project of Shanghai Education Committee (09ZZ158), Leading Academic Discipline Project of Shanghai Municipal Government (S30501)
1. Control Science and Engineering Department, University of Shanghai for Science and Technology, Shanghai 200093, P. R. China
2. School of Science, Ningbo University of Technology, Ningbo 315016, P.R. China

Assume that the geometric center point and the mass center point of the robot are the same. The nonholonomic constraint is defined by

$$\dot{x}\sin\theta - \dot{y}\cos\theta = 0$$

where (x, y) denotes the position P of the center of mass, θ is the angle between X axis and X_1 axis with a positive anticlockwise direction. By this formula, the kinematics of the robot can be modeled by the following differential equations

$$\begin{cases} \dot{x} = \nu_1 \cos\theta \\ \dot{y} = \nu_1 \sin\theta \\ \dot{\theta} = \omega \end{cases} \tag{1}$$

where ν_1 is the forward velocity, while ω is the angular velocity of the robot.

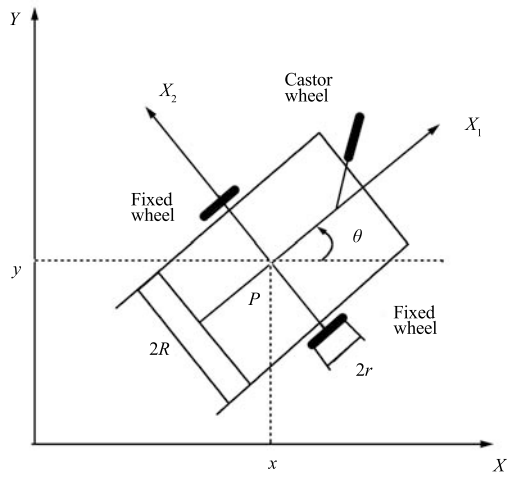

Fig. 1 Tricycle-type mobile robot

The system (1) can be written in matrix as follows:

$$\dot{\boldsymbol{q}} = S(\boldsymbol{q})\boldsymbol{v}(t) \tag{2}$$

where $\boldsymbol{v}(t) = [\nu_1, \omega]^{\mathrm{T}}$ and $S(\boldsymbol{q})$ is expressed as

$$S(\boldsymbol{q}) = \begin{bmatrix} \cos\theta & 0 \\ \sin\theta & 0 \\ 0 & 1 \end{bmatrix} \tag{3}$$

with $\boldsymbol{q} = (x, y, \theta)^{\mathrm{T}}$.

According to the Euler-Lagrangian formulation, the nonholonomic dynamic model of the mobile robot can be described as

$$M(\boldsymbol{q})\ddot{\boldsymbol{q}} + C(\boldsymbol{q}, \dot{\boldsymbol{q}})\dot{\boldsymbol{q}} + \boldsymbol{\tau}_d = B(\boldsymbol{q})\boldsymbol{\tau} + A^{\mathrm{T}}(\boldsymbol{q})\lambda \tag{4}$$

where $M(\boldsymbol{q}) \in \mathbf{R}^{3\times 3}$ is a positive definite symmetric inertial matrix, λ is a Lagrange multiplier which expresses the constraint force, $C(\boldsymbol{q}, \dot{\boldsymbol{q}}) \in \mathbf{R}^{3\times 3}$ represents of centripetal and Coriolis torque, $B(\boldsymbol{q}) \in \mathbf{R}^{3\times 2}$ is an input transformation matrix, $\boldsymbol{\tau}_d \in \mathbf{R}^2$ denotes bounded unknown disturbances including unstructured unmodelled dynamics, $\boldsymbol{\tau} \in \mathbf{R}^2$ is the torque applied to the right and left wheels.

Differentiating both sides of (2) and substituting it into (4), pre-multiplying both sides by $S^{\mathrm{T}}(\boldsymbol{q})$, one obtains

$$M_1(\boldsymbol{q})\dot{\boldsymbol{v}} + C_1(\boldsymbol{q}, \dot{\boldsymbol{q}})\boldsymbol{v} + \bar{\boldsymbol{\tau}}_d = B_1(\boldsymbol{q})\boldsymbol{\tau} \tag{5}$$

where $M_1(\boldsymbol{q}) = S^{\mathrm{T}}(\boldsymbol{q})M(\boldsymbol{q})S(\boldsymbol{q})$, $C_1(\boldsymbol{q}, \dot{\boldsymbol{q}}) = S^{\mathrm{T}}(M\dot{S} + CS)$, $\bar{\boldsymbol{\tau}}_d = S^{\mathrm{T}}(\boldsymbol{q})\boldsymbol{\tau}_d$, $B_1(\boldsymbol{q}) = S^{\mathrm{T}}(\boldsymbol{q})B(\boldsymbol{q})$. System (5) is more appropriate for controller design as the constraint λ has been eliminated from dynamic equation (4). In order to completely actuate the nonholonomic system, $B_1(\boldsymbol{q})$ is assumed to be a full rank matrix.

Assumption 1. $\| \bar{\boldsymbol{\tau}}_d \|$ is bounded by a known scalar, i.e., $\| \bar{\boldsymbol{\tau}}_d \| \leq d_B$, where $\| \cdot \|$ is usually called Euclid norm, and d_B is a known constant.

1.2 Kinematic and dynamic models with monocular camera

Generally, (x, y) can be obtained from the encoders of motors and other sensors such as ultrasonic sensors, infrared sensors, etc. However, for complex environments, it is difficult to implement this strategy. Instead, we will take advantage of the vision information to deal with this challenge.

In this paper, a camera is used to measure the position (x, y) and determine the desired target. A key strategy is that the error between the mass center point of the robot and its desired point in the image frame can be used in the closed-loop feedback control of the robot. As for the angle θ, it can be obtained easily from the angle sensor. Therefore, θ is still included in the error model.

Firstly, we consider that the movement of the mobile robot can be measured by using a fixed camera.

In Fig. 2, it is assumed that a pinhole camera is fixed to the ceiling, the mobile robot mentioned in Fig. 1 is under the camera, the camera plane and the robot plane are parallel. There are three coordinate frames, namely the inertial frame X-Y-Z, the camera frame x - y - z and the image frame u - o_1 - v. Assume that the x - y plane of the camera frame is parallel with the plane of the image coordinate plane. C is the crossing point between the optical axis of the camera and X-Y plane. Its coordinate relative to X-Y plane is (c_x, c_y). The coordinate of the intersection of the optical axis with the image plane is denoted by (O_{c1}, O_{c2}). (x, y) is the coordinate of the mass center P of the robot with respective to X-Y plane. Suppose that (x_m, y_m) is the coordinate of (x, y) relative to the image frame. In this work, the perspective camera model is used to obtain that[17]

$$\begin{bmatrix} x_m \\ y_m \end{bmatrix} = \begin{bmatrix} \alpha_1 & 0 \\ 0 & \alpha_2 \end{bmatrix} R(\theta) \left[\begin{bmatrix} x \\ y \end{bmatrix} - \begin{bmatrix} c_x \\ c_y \end{bmatrix} \right] + \begin{bmatrix} O_{c1} \\ O_{c2} \end{bmatrix} \tag{6}$$

where α_1 and α_2 are constants, which are dependent on the depth information, focal length, scalar factors along u axis and v axis respectively. In (6)

$$R(\theta) = \begin{bmatrix} \cos\theta_0 & \sin\theta_0 \\ -\sin\theta_0 & \cos\theta_0 \end{bmatrix}$$

where θ_0 denotes the angle between y axis and X axis with a positive anticlockwise orientation.

Differentiating (6) with respect to time and using (1), we obtain the camera-object visual servoing kinematic model

$$\begin{bmatrix} \dot{x}_m \\ \dot{y}_m \\ \dot{\theta} \end{bmatrix} = \begin{bmatrix} \nu_1\alpha_1\cos(\theta - \theta_0) \\ \nu_1\alpha_2\sin(\theta - \theta_0) \\ \omega \end{bmatrix} \tag{7}$$

If α_1, α_2 and θ_0 are all known, (7) can be reduced to a common nonholonomic chained form by using coordinate transformation. Its stabilizing problem can be addressed by lots of methods[2−4]. But, in practice, α_1, α_2, and θ_0 need to be measured. As usual, these parameters can be

obtained by using calibrating methods, at the expense of considerable calculation on calibration. To overcome this computational burden, we propose a novel solution to adaptive stabilization of system (7) without calibration.

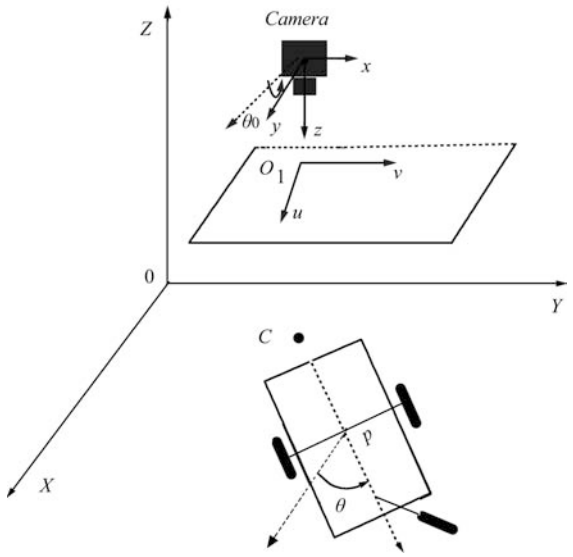

Fig. 2 Wheeled mobile robot below monocular camera

2 Adaptive controller design

2.1 Stabilizing controller design of the kinematic model

Assumption 2. θ_0 is known, $\alpha_1 = \alpha_2 = \alpha$ are unknown, $\underline{\alpha} \le \alpha \le \overline{\alpha}$, $\underline{\alpha}$ and $\overline{\alpha}$ are positive known constants.

Remark 1. $\alpha_1 = \alpha_2 = \alpha$ means that the scalar factor along u axis is the same as that one along v axis. Some CCD cameras are made like this. The assumption $\underline{\alpha} \le \alpha \le \overline{\alpha}$ is not strong. Commonly, the upper and lower bounds of the scalar factor, the depth and the focal length can be estimated in advance.

Based on Assumption 2 and replacing $\theta - \theta_0$ by θ in system (7), we have

$$\begin{bmatrix} \dot{x}_m \\ \dot{y}_m \\ \dot{\theta} \end{bmatrix} = \begin{bmatrix} \nu_1 \alpha \cos\theta \\ \nu_1 \alpha \sin\theta \\ \omega \end{bmatrix} \tag{8}$$

According to the transformation (6), the dynamic subsystem (5) is written as

$$M_2(\boldsymbol{q}_m)\dot{\boldsymbol{v}} + C_2(\boldsymbol{q}_m, \dot{\boldsymbol{q}}_m)\boldsymbol{v} + \bar{\boldsymbol{\tau}}_d = B_2(\boldsymbol{q}_m)\boldsymbol{\tau} \tag{9}$$

with $\boldsymbol{q}_m = (x_m, y_m, \theta)^{\mathrm{T}}$.

According to [18], we know that the coefficients M_1, C_1, B_1 of dynamic equation (5) are only dependent on angle θ and have nothing to do with x and y. However, the transformation (6) is independent of angle θ. So, we have

$$M_2(\boldsymbol{q}_m) = M_1(\boldsymbol{q})$$

$$C_2(\boldsymbol{q}_m, \dot{\boldsymbol{q}}_m) = C_1(\boldsymbol{q}, \dot{\boldsymbol{q}})$$

$$B_2(\boldsymbol{q}_m) = B_1(\boldsymbol{q})$$

Set

$$\boldsymbol{h} = \begin{bmatrix} z_1 \\ z_2 \\ \theta \end{bmatrix} = \begin{bmatrix} \cos\theta & \sin\theta & 0 \\ \sin\theta & -\cos\theta & 0 \\ 0 & 0 & 1 \end{bmatrix} \begin{bmatrix} x_m \\ y_m \\ \theta \end{bmatrix}$$

then (8) yields

$$\begin{cases} \dot{z}_1 = -\omega z_2 + \alpha \nu_1 \\ \dot{z}_2 = \omega z_1 \\ \dot{\theta} = \omega \end{cases} \tag{10}$$

The dynamic subsystem (9) correspondingly becomes

$$M_3(\boldsymbol{h})\dot{\boldsymbol{v}} + C_3(\boldsymbol{h}, \dot{\boldsymbol{h}})\boldsymbol{v} + \bar{\boldsymbol{\tau}}_d = B_3(\boldsymbol{h})\boldsymbol{\tau} \tag{11}$$

where

$$M_3(\boldsymbol{h}) = M_2(\boldsymbol{q}_m)|_{\boldsymbol{q}_m = T^{-1}\boldsymbol{h}}$$

$$C_3(\boldsymbol{h}, \dot{\boldsymbol{h}}) = C_2(\boldsymbol{q}_m, \dot{\boldsymbol{q}}_m)|_{\boldsymbol{q}_m = T^{-1}\boldsymbol{h}}$$

$$B_3(\boldsymbol{h}) = B_2(\boldsymbol{q}_m)|_{\boldsymbol{q}_m = T^{-1}\boldsymbol{h}}$$

and

$$T = \begin{bmatrix} \cos\theta & \sin\theta & 0 \\ \sin\theta & -\cos\theta & 0 \\ 0 & 0 & 1 \end{bmatrix}$$

Due to the nonsingularity of S and T, the transformed dynamic system (11) has the same properties as (4) or (5). Some interesting properties of the dynamic model (11) are listed below:

Property 1. $M_3(\boldsymbol{h})$ is a positive definite symmetric matrix.

Property 2. $\dot{M}_3 - 2C_3$ is skew-symmetric.

Property 3. For any differentiable vector $\boldsymbol{\xi}$,

$$M_3(\boldsymbol{h})\dot{\boldsymbol{\xi}} + C_3(\boldsymbol{h}, \dot{\boldsymbol{h}})\boldsymbol{\xi} = Y(\boldsymbol{h}, \dot{\boldsymbol{h}}, \boldsymbol{\xi}, \dot{\boldsymbol{\xi}})\boldsymbol{p} \tag{12}$$

where the regressor matrix $Y(\boldsymbol{h}, \dot{\boldsymbol{h}}, \boldsymbol{\xi}, \dot{\boldsymbol{\xi}})$ is a known matrix of $\boldsymbol{h}$, $\dot{\boldsymbol{h}}$, $\boldsymbol{\xi}$, and $\dot{\boldsymbol{\xi}}$, while $\boldsymbol{p}$ is an inertia parameter vector of the system.

As a basis of the full dynamic system study, let us first neglect the part of dynamics and consider the kinematic stabilization problem of system (10) only. From [13], the robot kinematic stabilizing control law $\boldsymbol{v}_d = (\nu_{1d}, \omega_d)^{\mathrm{T}}$ for system (10) is given below:

$$\nu_{1d} = -\mathrm{k}_2\eta + \hat{\varphi} z_2(\cos t + \omega_d),\ \omega_d = -\mathrm{k}_1(\theta + \chi) \tag{13}$$

where k_1 and k_2 denote the positive constant control gains, and η and χ are auxiliary signals defined as follows:

$$\eta = z_1 - z_2 \sin t,\quad \chi = (\eta + z_2 \sin t)(z_2 - \eta \sin t) \tag{14}$$

In (13), $\hat{\varphi}(t)$ denotes a dynamic estimated value of $\varphi = \frac{1}{\alpha}$, the parameter error signal $\tilde{\varphi}$ is defined by $\tilde{\varphi} = \varphi - \hat{\varphi}$, the parameter adaptive law will be given later.

To design the torque input $\boldsymbol{\tau}$ for the complete dynamic systems (10) and (11), which will make the output $\boldsymbol{v}(t)$ of the dynamic system tend to the desired velocity $\boldsymbol{v}_d$, the auxiliary velocity tracking error signal denoted by $\boldsymbol{e}(t) \in \mathbf{R}^2$ is defined as follows:

$$\boldsymbol{e} = [e_1, e_2]^{\mathrm{T}} = \boldsymbol{v} - \boldsymbol{v}_d \tag{15}$$

After substituting (13), (15) into (10), the following closed-loop error system for z_1, z_2, θ is obtained.

$$\begin{cases} \varphi\dot{z}_1 = -\mathrm{k}_2\eta + \hat{\varphi}z_2(\cos t + \omega_d) - \varphi z_2(\omega_d + e_2) + e_1 \\ \dot{z}_2 = -\mathrm{k}_1 z_1(\theta + \chi) + e_2 z_1 \\ \dot{\theta} = -\mathrm{k}_1(\theta + \chi) + e_2 \end{cases} \tag{16}$$

2.2 Stabilizing controller design of the dynamic system

In this subsection, we utilize the dynamic model given by (11) to design a control torque input $\boldsymbol{\tau}$ to stabilize systems (10) and (11) when the inertia parameter vector $\boldsymbol{p}$, the camera parameter α are unknown and unknown disturbance $\boldsymbol{\tau}_d$ exists.

Differentiating (15) and using the result in (11), the robot dynamics using the velocity tracking error can be rewritten as

$$M_3(\boldsymbol{h})\dot{\boldsymbol{e}} + C_3(\boldsymbol{h}, \dot{\boldsymbol{h}})\boldsymbol{e} + Y_c\boldsymbol{p} + \bar{\boldsymbol{\tau}}_d = B_3(\boldsymbol{h})\boldsymbol{\tau} \tag{17}$$

where $Y_c\boldsymbol{p}$ is defined as

$$Y_c\boldsymbol{p} = M_3\dot{\boldsymbol{v}}_d + C_3\boldsymbol{v}_d \tag{18}$$

where $Y_c(\cdot) \in \mathbf{R}^{2\times s}$ denotes the known desired regression matrix, and $\boldsymbol{p}$ is defined in (12).

Based on the subsequent stability proof and the regulation of $\boldsymbol{e}(t)$, we design the control torque input $\boldsymbol{\tau}(t)$ as follows:

$$\boldsymbol{\tau}(t) = B_3^{-1}\bar{\boldsymbol{\tau}} \tag{19}$$

where $\bar{\boldsymbol{\tau}} \in \mathbf{R}^2$ is an auxiliary control signal designed as shown in the following:

$$\begin{cases} \bar{\boldsymbol{\tau}} = Y_c\hat{\boldsymbol{p}} - \boldsymbol{u}_{s1} - \begin{bmatrix} k_{d1}e_1 + \eta \\ k_{d2}e_2 + \hat{\varphi}((\theta + \chi) - z_2\eta) \end{bmatrix} \\ \boldsymbol{u}_{s1} = d_B \cdot \mathrm{sgn}(\boldsymbol{e}) = d_B \cdot [\mathrm{sgn}(e_1), \mathrm{sgn}(e_2)]^{\mathrm{T}} \end{cases} \tag{20}$$

where k_{d1} and k_{d2} are positive constant control gains, the parameter update laws for $\hat{\boldsymbol{p}}$ and $\hat{\varphi}$ are designed as follows:

$$\dot{\hat{\boldsymbol{p}}} = -\Gamma Y_c^{\mathrm{T}}\boldsymbol{e} \tag{21}$$

$$\dot{\hat{\varphi}} = \Lambda[e_2(\theta + \chi) - \eta z_2(\cos t + \omega_d + e_2)] \tag{22}$$

where Γ and Λ are positive definite gain matrices. After substituting (19) and (20) into (17), the closed loop error dynamics for $\boldsymbol{e}(t)$ can be expressed as

$$M_3\dot{\boldsymbol{e}} = -C_3\boldsymbol{e} - Y_c\tilde{\boldsymbol{p}} - \bar{\boldsymbol{\tau}}_d - d_B \cdot \mathrm{sgn}(\boldsymbol{e}) - \begin{bmatrix} k_{d1}e_1 + \eta \\ k_{d2}e_2 + \hat{\varphi}((\theta + \chi) - z_2\eta) \end{bmatrix} \tag{23}$$

where the parameter error signal denoted by $\tilde{\boldsymbol{p}}$ is defined as:

$$\tilde{\boldsymbol{p}} = \boldsymbol{p} - \hat{\boldsymbol{p}}$$

3 Stability analysis

Theorem 1. Under Assumptions 1 and 2, the control inputs given in (13) $\sim$ (15), (19) $\sim$ (22) for systems (10) and (11) ensure that system (10) can be uniformly globally asymptotically stabilized to zero in the sense that

$$\lim_{t\to\infty} z_1(t), z_2(t), \theta(t), e_1(t), e_2(t) = 0 \tag{24}$$

Proof. To prove Theorem 1, we consider a Lyapunov function candidate

$$V = \frac{1}{2\alpha}(\eta^2 + z_2^2 + \theta^2) + \frac{1}{2}\Lambda^{-1}\tilde{\varphi}^2 + \frac{1}{2}\boldsymbol{e}^{\mathrm{T}}M_3\boldsymbol{e} + \frac{1}{2}\tilde{\boldsymbol{p}}^{\mathrm{T}}\Gamma^{-1}\tilde{\boldsymbol{p}} \tag{25}$$

We notice that, utilizing (13) and the first equation of (16), we have

$$\varphi\dot{\eta} = [-\mathrm{k}_2\eta - \tilde{\varphi}\omega_d z_2 - \varphi z_2 e_2 - \varphi z_1 \sin t(\omega_d + e_2) + e_1] - \tilde{\varphi}z_2\cos t \tag{26}$$

After taking the time derivative of (25) and making the appropriate substitutions from (16), (23), (26) and by Property 2, we have

$$\begin{aligned} \dot{V} &= \varphi(\eta\dot{\eta} + z_2\dot{z}_2 + \theta\dot{\theta}) + \tfrac{1}{2}\boldsymbol{e}^{\mathrm{T}}\dot{M}_3\boldsymbol{e} + \boldsymbol{e}^{\mathrm{T}}M_3\dot{\boldsymbol{e}} + \tilde{\boldsymbol{p}}^{\mathrm{T}}\Gamma^{-1}\dot{\tilde{\boldsymbol{p}}} + \Lambda^{-1}\tilde{\varphi}\dot{\tilde{\varphi}} \\ &= -k_2\eta^2 - \varphi k_1(\theta + \chi)(\theta + z_1z_2 - z_1\eta\sin t) + \varphi[-\eta z_2e_2 - \eta z_1e_2\sin t + z_1z_2e_2 + \theta e_2] - \tilde{\varphi}z_2\eta(\cos t + \omega_d) + e_1\eta + \tfrac{1}{2}\boldsymbol{e}^{\mathrm{T}}\dot{M}_3\boldsymbol{e} + \boldsymbol{e}^{\mathrm{T}}M_3\dot{\boldsymbol{e}} + \tilde{\boldsymbol{p}}^{\mathrm{T}}\Gamma^{-1}\dot{\tilde{\boldsymbol{p}}} + \Lambda^{-1}\tilde{\varphi}\dot{\tilde{\varphi}} \\ &= -k_2\eta^2 - \varphi k_1(\theta + \chi)^2 + \varphi[-\eta z_2e_2 + (\theta + \chi)e_2] + e_1\eta - \tilde{\varphi}\eta z_2(\cos t + \omega_d) + \Lambda^{-1}\tilde{\varphi}\dot{\tilde{\varphi}} + \tilde{\boldsymbol{p}}^{\mathrm{T}}\Gamma^{-1}\dot{\tilde{\boldsymbol{p}}} - \boldsymbol{e}^{\mathrm{T}}Y_c\tilde{\boldsymbol{p}} - \boldsymbol{e}^{\mathrm{T}}\bar{\tau}_d - \boldsymbol{e}^{\mathrm{T}}d_B \cdot \mathrm{sgn}(\boldsymbol{e}) - \boldsymbol{e}^{\mathrm{T}}\begin{bmatrix} k_{d1}e_1 + \eta \\ k_{d2}e_2 + \hat{\varphi}((\theta + \chi) - z_2\eta) \end{bmatrix} \\ &= -k_2\eta^2 - \varphi k_1(\theta + \chi)^2 - k_{d1}e_1^2 - k_{d2}e_2^2 - \boldsymbol{e}^{\mathrm{T}}\bar{\boldsymbol{\tau}}_d - \boldsymbol{e}^{\mathrm{T}}d_B \cdot \mathrm{sgn}(\boldsymbol{e}) \end{aligned} \tag{27}$$

Since

$$\begin{aligned} -\boldsymbol{e}^{\mathrm{T}}\bar{\boldsymbol{\tau}}_d - \boldsymbol{e}^{\mathrm{T}}d_B \cdot \mathrm{sgn}(\boldsymbol{e}) &= -[d_B\boldsymbol{e}^{\mathrm{T}}\mathrm{sgn}(\boldsymbol{e}) + \boldsymbol{e}^{\mathrm{T}}\bar{\boldsymbol{\tau}}_d] \le \\ &\quad -[d_B\|\boldsymbol{e}\| - \|\bar{\boldsymbol{\tau}}_d\|\,\|\boldsymbol{e}\|] \le 0 \end{aligned} \tag{28}$$

we have

$$\dot{V} \le -k_2\eta^2 - \varphi k_1(\theta + \chi)^2 - k_{d1}e_1^2 - k_{d2}e_2^2 \le 0 \tag{29}$$

From the expression of (29), we know that the function $V(t)$ never increases its value so that it converges to a nonnegative number, thus, $V(t)$ is bounded. According to the definition (25), bounded $V(t)$ directly implies that the $e_1(t), e_2(t)$, $\eta(t)$, $\tilde{\boldsymbol{p}}$, $\tilde{\varphi}$, θ, and z_2 are all bounded. Thus, $\hat{\boldsymbol{p}}$ and $\hat{\varphi}$ are bounded as well. Furthermore, e_1, e_2, η, and $(\theta + \chi) \in L_2$ can be obtained due to (29) and the boundedness of $V(t)$. From (14), (16), (23) and the boundedness of α, we have $\dot{\theta}$, $\dot{z}_1$, $\dot{z}_2$, $\dot{e}_1$, $\dot{e}_2$, and $(\dot{\theta} + \dot{\chi})$ are all bounded, thus, e_1, e_2, η, and $(\theta + \chi)$ are uniformly continuous. Due to the Barbalat Lemma[19], we have

$$\lim_{t\to\infty} e_1(t), e_2(t), \eta(t), (\theta + \chi)(t) = 0 \tag{30}$$

The result in (30) can be used in conjunction with the closed-loop dynamics for $\theta(t)$ and $z_2(t)$ given in (16) and the control input of (13) to determine that

$$\lim_{t\to\infty} \dot{\theta}(t), \omega_d(t), \dot{z}_2(t) = 0 \tag{31}$$

The results in (30) and (31) can be used to determine that the bracketed term of (26) goes to zero as $t \to \infty$; therefore, since $\tilde{\varphi}$ and z_2 are uniformly continuous and $\eta(t)$ has a finite limit as $t \to \infty$, the extended Barbalat lemma can be invoked to prove that

$$\lim_{t\to\infty} \dot{\eta}(t) = 0 \tag{32}$$

After taking the time derivative of $\theta + \chi$, according to (14) and (16), the following resulting expression can be obtained:

$$\frac{\mathrm{d}}{\mathrm{d}t}[\theta + \chi] = [-k_1(\theta + \chi) + e_2 + \phi(t)] + z_2^2 \cos t \tag{33}$$

where the auxiliary signal $\phi(t)$ is defined as follows:

$$\begin{aligned}\phi(t) \ =& (\eta + z_2 \sin t)(\dot{z}_2 - \dot{\eta}\sin t - \eta\cos t) + \\ & z_2(\dot{\eta} + \dot{z}_2 \sin t) - \eta \sin t(\dot{\eta} + \dot{z}_2 \sin t + z_2 \cos t)\end{aligned} \tag{34}$$

Based on (30)$\sim$(32), we have

$$\lim_{t\to\infty} \phi(t) = 0 \tag{35}$$

From (30) and (35), the bracketed term of (33) also goes to zero as $t \to \infty$. Since z_2 is uniformly continuous and $\theta + \chi$ has a finite limit as $t \to \infty$, the extended Barbalat lemma can be utilized to conclude that $\lim_{t\to\infty} z_2^2 \cos t = 0$, thus,

$$\lim_{t\to\infty} z_2^2 \cos^2 t = 0 \tag{36}$$

We notice that

$$(z_2^2 \cos t)' = 2z_2\dot{z}_2 \cos t - z_2^2 \sin t \tag{37}$$

By using the extended Barbalat lemma again, we obtained that $\lim_{t\to\infty} z_2^2 \sin t = 0$, thus

$$\lim_{t\to\infty} z_2^2 \sin^2 t = 0 \tag{38}$$

Considering (36), we obtain that

$$\lim_{t\to\infty} z_2^2(\sin^2 t + \cos^2 t) = \lim_{t\to\infty} z_2^2(t) = 0 \tag{39}$$

Hence,

$$\lim_{t\to\infty} z_2(t) = 0 \tag{40}$$

Based on the previous facts (14) and (30), we can obtain

$$\lim_{t\to\infty} z_1(t) = 0 \tag{41}$$

By utilizing (30), (40), (41), and the definitions introduced in (14), the following result can be obtained

$$\lim_{t\to\infty} z_1(t), z_2(t), \theta(t), e_1(t), e_2(t) = 0 \tag{42}$$

□

Remark 2. The proposed adaptive robust algorithm can guarantee the asymptotical stability of the system. The bounded disturbance can be completely suppressed by $-d_B \cdot \mathrm{sgn}(\boldsymbol{e})$. However, this may bring chattering into the system since the discontinuous surfaces exist. To overcome the chattering problem, a smoothly sliding mode control law taking into account the boundary is introduced:

$$\boldsymbol{u}_{s1} = \begin{cases} d_B \cdot \mathrm{sgn}(\boldsymbol{e}), & \text{if } \|\boldsymbol{e}\| > \delta(t) \\ d_B \frac{\boldsymbol{e}}{\delta}, & \text{if } \|\boldsymbol{e}\| \le \delta(t) \end{cases} \tag{43}$$

where $\delta(t)$ is a positive integration function on $[0, +\infty)$ such that

$$\int_0^{+\infty} \delta(\sigma)\mathrm{d}\sigma \le \mu$$

with μ being a nonnegative constant.

If $\|\boldsymbol{e}\| > \delta(t)$, then

$$\dot{V} \le -k_2\eta^2 - \varphi k_1(\theta + \chi)^2 - k_{d1}e_1^2 - k_{d2}e_2^2 \le 0 \tag{44}$$

If $\|\boldsymbol{e}\| \le \delta(t)$, then

$$\begin{aligned}-\boldsymbol{e}^{\mathrm{T}}\bar{\boldsymbol{\tau}}_d - \boldsymbol{e}^{\mathrm{T}}\boldsymbol{u}_{s1} =& -\boldsymbol{e}^{\mathrm{T}}\bar{\boldsymbol{\tau}}_d - \tfrac{d_B\boldsymbol{e}^{\mathrm{T}}\boldsymbol{e}}{\delta} \le d_B\|\boldsymbol{e}\| - \tfrac{d_B\|\boldsymbol{e}\|^2}{\delta} \le \\ & d_B\|\boldsymbol{e}\| + d_B\|\boldsymbol{e}\| \le 2d_B\delta\end{aligned} \tag{45}$$

Thus, we have

$$\dot{V} \le -k_2\eta^2 - \varphi k_1(\theta + \chi)^2 - k_{d1}e_1^2 - k_{d2}e_2^2 + 2d_B\delta \tag{46}$$

So, when we choose the smoothly variable structure control law $\boldsymbol{u}_{s1}$ in (43), formula (46) is always valid.

Now, we can prove that the control inputs (13) and (20) with $\boldsymbol{u}_{s1}$ as defined in (43) can guarantee that the conclusion of Theorem 1 can be obtained. By integrating both sides of (46), it is seen that $V(t) \le V(0) + 2d_B\int_0^t \delta(\sigma)\mathrm{d}\sigma \le V(0) + \mu$. Thus, $\eta,\ z_2,\ \theta,\ e_1,\ e_2,\ \tilde{\varphi}$ and $\tilde{\boldsymbol{p}}$ are all bounded, and $(\theta + \chi),\ \hat{\varphi}$ and $\hat{\boldsymbol{p}}$ are all bounded as well. In view of (14), (16) and (23), we obtain that $(\dot{\theta} + \dot{\chi}),\ \dot{\eta},\ \dot{e}_1$, and $\dot{e}_2$ are all bounded. Hence, $(\theta+\chi),\ \eta,\ e_1$, and e_2 are uniformly continuous. Notice that

$$k_1\varphi(\theta+\chi)^2 + k_2\eta^2 + k_{d1}e_1^2 + k_{d2}e_2^2 \le -\dot{V}(t) + 2d_B\delta(t) \tag{47}$$

By integrating both sides of (47), we can see that $(\theta + \chi),\ \eta,\ e_1$, and $e_2 \in L_2$. By using Barbalat lemma, we can obtain

$$\lim_{t\to\infty} \eta, \theta + \chi, e_1, e_2 = 0$$

Same process to the proof of Theorem 1, we can prove that $\lim_{t\to\infty} z_1(t), z_2(t), \theta(t), e_1(t), e_2(t) = 0$. Here omitted due to the limited space.

Remark 3. The examples of time-varying boundary layer $\delta(t)$ are required to satisfy $\int_0^{+\infty}\delta(\sigma)\mathrm{d}\sigma \le \mu$, for instance, exponential function e^{-t}, $e^{-(1+t)}$; power function $\frac{1}{t^n}$, $\frac{1}{(1+t)^n}$, $n > 1$.

4 Simulation results

For the mobile robot system considered here, according to [20], the dynamic equation parameters of (4) can be given as

$$M(\boldsymbol{q}) = \begin{bmatrix} m & 0 & 0 \\ 0 & m & 0 \\ 0 & 0 & I \end{bmatrix}, \quad C(\boldsymbol{q}, \dot{\boldsymbol{q}}) = \begin{bmatrix} 0 & 0 & 0 \\ 0 & 0 & 0 \\ 0 & 0 & 0 \end{bmatrix}$$

$$B(\boldsymbol{q}) = \frac{1}{r}\begin{bmatrix} \cos\theta & \cos\theta \\ \sin\theta & \sin\theta \\ R & -R \end{bmatrix}$$

where $2R$ is the width of the mobile robot and r is the radius of the wheel, m is the mass of the mobile robot and I is its inertia moment around the vertical axis at point P.

According to the transformations of Sections 1 and 2, we have

$$M_3(\boldsymbol{h}) = \begin{bmatrix} m & 0 \\ 0 & I \end{bmatrix}, \quad C_3(\boldsymbol{h}, \dot{\boldsymbol{h}}) = \begin{bmatrix} 0 & 0 \\ 0 & 0 \end{bmatrix}$$

$$B_3(\boldsymbol{h}) = \frac{1}{r} \begin{bmatrix} 1 & 1 \\ R & -R \end{bmatrix}$$

The robot regressor Y_c and the inertia parameter vector $\boldsymbol{p}$ can be selected as $Y_c = \mathrm{diag}\{\dot{\nu}_{1d}, \dot{\omega}_d\}$, $\boldsymbol{p} = (m, I)^{\mathrm{T}}$.

Case 1. The simulation is implemented for the controllers defined in (13) and (20) with $\boldsymbol{u}_{s1} = d_B \cdot \mathrm{sgn}(\boldsymbol{e})$ being used. The corresponding closed loop systems are written by (16) and (23). Take $\underline{\alpha} = 0.5, \overline{\alpha} = 2$, $\frac{1}{\varphi} = \alpha = 1$, $m = 5\,\mathrm{kg}$, $I = 5\,\mathrm{kg} \cdot \mathrm{m}^2$, $R = 1\,\mathrm{m}$, $r = 0.1\,\mathrm{m}$. The parameters of the controller are chosen as $k_1 = 5, k_2 = 2$, $k_{d1} = k_{d2} = 20$, $d_B = 2$, and the gains $\Gamma = \mathrm{diag}\{10, 10\}$, $\Lambda = 5$. The external disturbance $\bar{\boldsymbol{\tau}}$ is a random number in the range $[-1, 1]^{\mathrm{T}}$ which is added to verify the robustness of the closed-loop systems.

The simulation results are shown in Figs. 3 $\sim$ 7, respectively. From Figs. 3 and 4, we can see that the posture errors z_1, z_2, θ and velocity errors e_1, e_2 asymptotically tend to zero. From Figs. 5 and 6, the estimates of the parameters $\hat{\boldsymbol{p}}$ and $\hat{\varphi}$ are bounded. As shown in Fig. 7, the control input $\boldsymbol{\tau} = (\tau_1, \tau_2)^{\mathrm{T}}$ is convergent to a small neighborhood of zero asymptotically. The effectiveness of the proposed controller is verified by the simulations.

In the simulation, as long as k_1 and k_2 are chosen positive, the errors are convergent. In the case, $k_1 = 5$ and $k_2 = 2$, the results are better. When one of k_1 and k_2 is chosen negative, the convergence of the errors could not be guaranteed. Generally, there are little effect caused by change of α.

Case 2. Now the smoothed sliding mode controller (13) and (20) with $\boldsymbol{u}_{s1}$ in (43) is used to see the performance of the system, where the boundary layer $\delta(t) = \frac{1}{(1+t)^3}$. For comparison, the parameters are chosen the same as in Case 1. Results are shown in Figs. 8 $\sim$ 12, respectively. From Fig. 12, we see that the chattering is removed and thus the proposed method is verified.

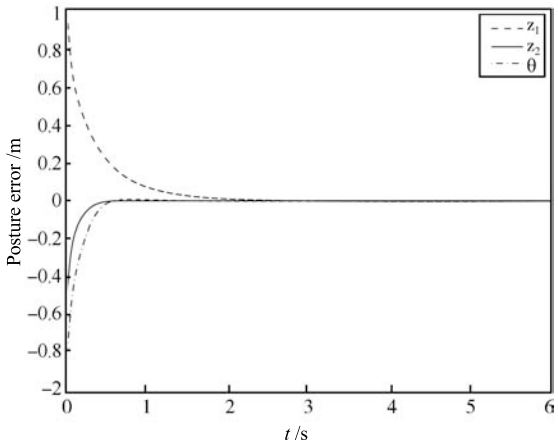

Fig. 3 The error states z_1, z_2, θ with respect to time

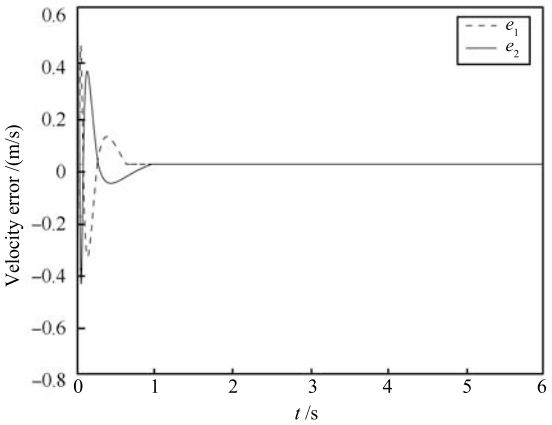

Fig. 4 The velocity errors e_1, e_2

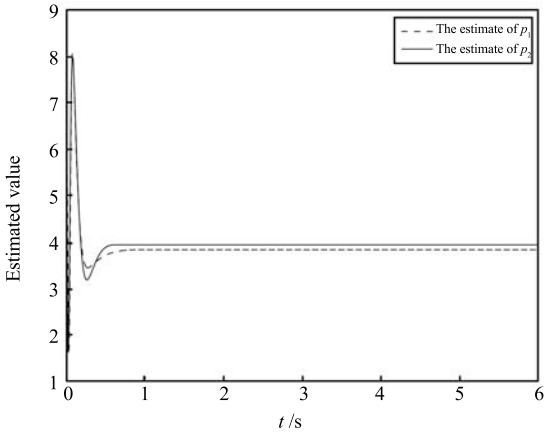

Fig. 5 The estimated parameters $\hat{p}_1, \hat{p}_2$

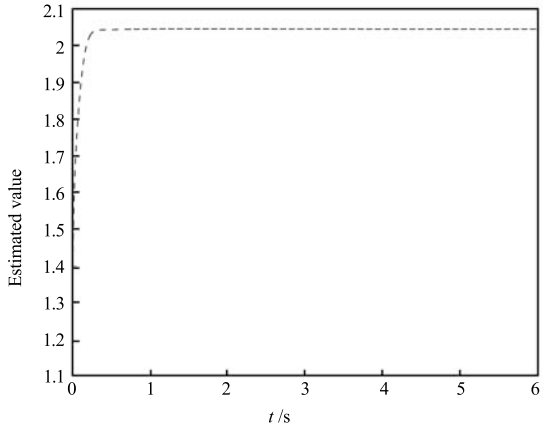

Fig. 6 The estimated parameter $\frac{1}{\hat{\alpha}} = \hat{\varphi}$

5 Conclusions

Based on sliding mode control and adaptive control techniques, a dynamic stabilizing controller has been proposed for nonholonomic mobile robots with unknown camera parameters, inertial parameters and disturbances of the dynamic system. The designed adaptive torque controller achieved global asymptotic stabilization and eliminated the need for integrating the nonlinear kinematic model to obtain the NMR Cartesian position for use in the closed-loop

control strategy. Hence, we believe that the vision-based control approach for NMRs holds the potential of higher performance. The closed-loop system stability and estimated error boundedness were proved by Lyapunov stability theory. Simulation results were presented to illustrate the performance of the proposed adaptive controller. Our future work will be devoted to relaxation of Assumption 2, and to the study of other nonholonomic mechanical systems.

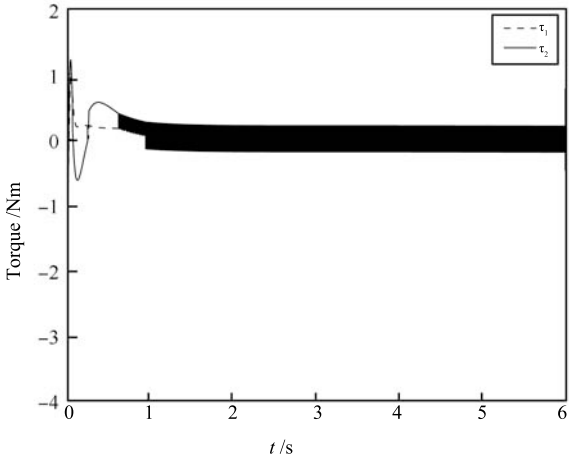

Fig. 7 The torques acted on the wheels

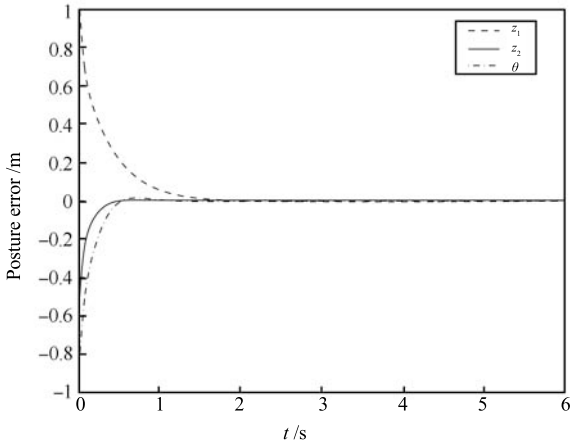

Fig. 8 The error states z_1, z_2, θ with respect to time

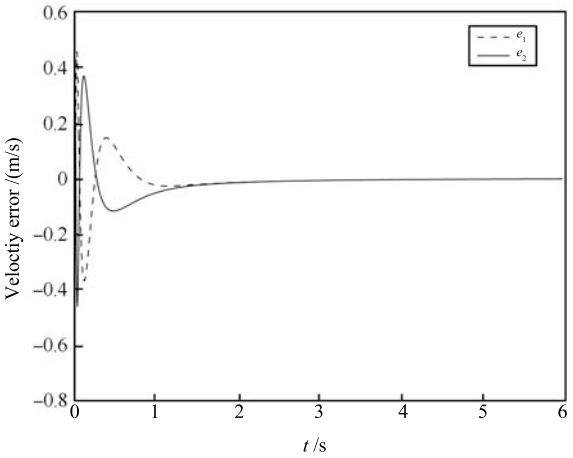

Fig. 9 The velocity errors e_1, e_2

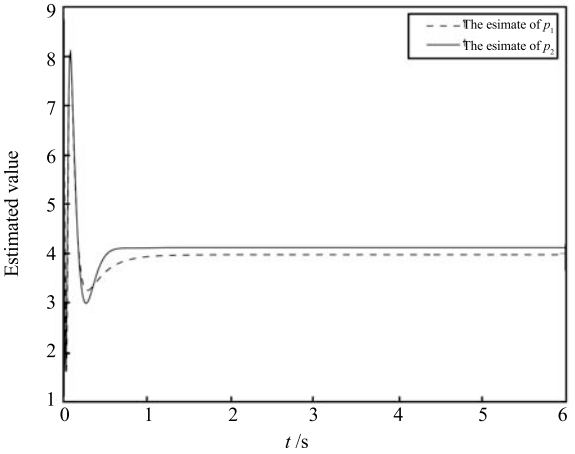

Fig. 10 The estimated parameters $\hat{p}_1, \hat{p}_2$

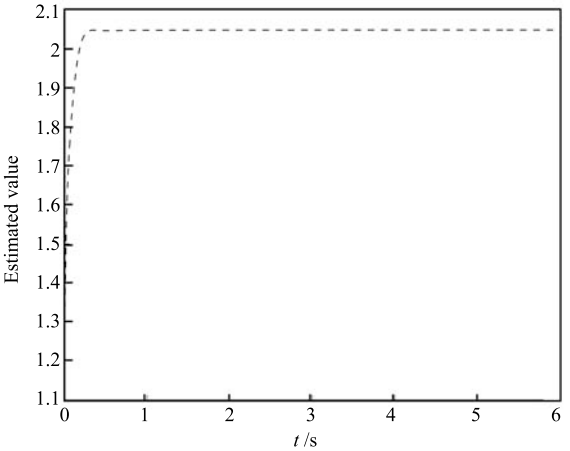

Fig. 11 The estimated parameter $\frac{1}{\hat{\alpha}} = \hat{\varphi}$

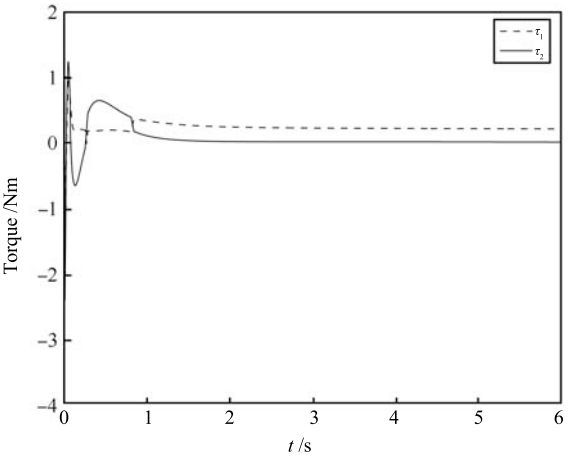

Fig. 12 The torques acted on the wheels

References

1 Brockett R W. Asymptotic stability and feedback stabilization. *Differential Geometric Control Theory*. Boston: Birkhauser, 1983. 181−191

2 Murray R M, Sastry S S. Nonholonomic motion planning: steering using sinusoids. *IEEE Transactions on Automatic Control*, 1993, **38**(5): 700−716

3 Sordalen O J, Egeland O. Exponential stabilization of nonholonomic chained systems. *IEEE Transactions on Automatic Control*, 1995, **40**(1): 35−49

4 Tian Y P, Li S H. Exponential stabilization of nonholonomic dynamic systems by smooth time-varying control. *Automatica*, 2002, **38**(7): 1139−1146

5 Astolfi A. Discontinuous control of nonholonomic systems. *Systems and Control Letters*, 1996, **27**(1): 37−45

6 Hu Y M, Ge S S, Su C Y. Stabilization of uncertain nonholonomic systems via time-varying sliding mode control. *IEEE Transactions on Automatic Control*, 2004, **49**(5): 757−763

7 Wang Qi-De, Wei Chun-Ling. Robust adaptive control of nonholonomic systems with nonlinear parameterization. *Acta Automatica Sinica*, 2007, **33**(4): 399−403

8 Wang C L, Mei Y C, Liang Z Y, Jia Q W. Dynamic feedback tracking control of non-holonomic mobile robots with unknown camera parameters. *Transactions of the Institute of Measurement and Control*, 2010, **32**(2): 155−169

9 Liang Zhen-Ying, Wang Chao-Li. Robust stabilization of nonholonomic chained form systems with uncertainties. *Acta AutomaticaSinica*, 2011, **37**(2): 129−142

10 Wang Y, Lang H X, Silva C W. A hybrid visual servo controller for robust grasping by wheeled mobile robots. *IEEE/ASME Transactions on Mechatronics*, 2010, **15**(5): 757−769

11 Hu G, MacKunis W, Gans N, Dixon W E, Chen J, Behal A, Dawson D. Homography-based visual servo control with imperfect camera calibration. *IEEE Transactions on Automatic Control*, 2009, **54**(6): 1318−1324

12 Chen J, Dixon W E, Dawson D M, McIntyre M. Homography-based visual servo tracking control of a wheeled mobile robot. *IEEE Transactions on Robotics*, 2006, **22**(2): 406−415

13 Fang Y C, Dixon W E, Dawson D M, Chawda P. Homography-based visual servo regulation of mobile robots. *IEEE Transactions on Systems, Man and Cybernetics, Part B: Cybernetics*, 2005, **35**(5): 1041−1050

14 Wang C L, Liang Z Y, Jia Q W. Dynamic feedback robust stabilization of nonholonomic mobile robots based on visual servoing. *Journal of Control Theory and Applications*, 2010, **8**(2): 139−144

15 Liu Y H, Wang H S, Wang C Y, Lam K K. Uncalibrated visual servoing of robots using a depth-independent interaction matrix. *IEEE Transactions on Robotics*, 2006, **22**(4): 804−817

16 Wang H S, Liu Y H, Zhou D X. Adaptive visual servoing using point and line features with an uncalibrated eye-in-hand camera. *IEEE Transactions on Robotics*, 2008, **24**(4): 843−857

17 Dixon W E, Dawson D M, Zergeroglu E, Behal A. Adaptive tracking control of a wheeled mobile robot via an uncalibrated camera system. *IEEE Transactions on Systems, Man and Cybernetics, Part B: Cybernetics*, 2001, **31**(3): 341−352

18 Campion G, Bastin G, Dandrea-Novel B. Structural properties and classification of kinematic and dynamic models of wheeled mobile robots. *IEEE Transaction on Robotics and Automation*, 1996, **22**(1): 47−62

19 Khalil H K. *Nonlinear Systems (Third Edition)*. New Jersey: Prentice Hall, 2001

20 Fierro R, Lewis F L. Control of a nonholonomic mobile robots: backstepping kinematics into dynamics. In: Proceedings of the 34th Conference on Decision and Control. New Orleans, USA: IEEE, 1995. 3805−3810

YANG Fang Ph. D. candidate at University of Shanghai for Science and Technology. She received her B. S. degree in 2002 and M. S. degree in 2005, both from Mathematics Department at Anhui University. Her research interests covers nonlinear system control, robust adaptive control, and robot dynamic and control. Corresponding author of this paper.
E-mail: liusha_02@163.com

WANG Chao-Li Professor in the Department of Control Science and Engineering, University of Shanghai for Science and Technology. He received his Ph. D. degree in control theory and engineering from Beijing University of Aeronautics and Astronautics in 1999. From 1999 to 2002, he worked as a postdoctoral research fellow with Robotics Laboratory of Chinese Academy of Sciences. His research interest covers nonlinear control, robust control, robot dynamics and control, visual servoing feedback control, and pattern identification.
E-mail: clclwang@126.com